

Local field enhancement in star-like sets of plasmon nanoparticles

Vladimir Poponin*

Nanophotonics Biosciences Inc., 1801 Bush Street, San Francisco, CA 94109, USA

Alexander Ignatov

General Physics Institute, 38 Vavilova str., 119991 Moscow, Russia

(Dated: September 8, 2018)

Abstract

We investigate the critical points of the near field intensity in the vicinity of dielectric bodies illuminated by the incident light. It is shown that in the electrostatic approximation there are no local maxima of the intensity outside dielectric surfaces and the only possible critical points are either local minima or saddle points. Using the boundary charge method we investigate numerically the field distribution around star-like sets of prolate spheroids. The field enhancement is shown to achieve a value of several hundreds at critical points outside the surfaces of spheroids.

PACS numbers: 78.67.-n, 68.37.Uv, 73.20.Mr

Keywords: Near-field optics, plasmon resonance

*Electronic address: v.poponin@att.net

I. INTRODUCTION

Progress in near-field optics is caused by development of both experimental technique and mathematical methods of calculations of the near-field structures. Near-field microscopy has been successfully used to overcome the diffraction limit and to achieve subwavelength resolution imaging of various surface structures [1]. Of particular interest is a phenomenon of localization and enhancement of the EM near field by metallic nanoparticles and clusters [2]. For the explanation of the phenomena of the Surface Enhanced Raman Scattering of particular interest are large local fields induced in close proximity or at the surfaces of nanoparticles [3, 4]. Mechanism of extraordinary Raman enhancement is still not completely understood. However, according to electromagnetic mechanism fields localized on surfaces of nanoparticles are responsible for extraordinary amplification of the Raman scattering. According to electromagnetic mechanism [5, 6, 7] the cross-section of Raman scattering is proportional to the fourth power of the local field. Therefore, even moderate enhancement of the local electromagnetic field results in the extraordinary amplification of the Raman scattering. Enhancement of the Raman cross section up to ten power fourteen was reported in literature thus allowing for single molecule Raman spectroscopy and detection [3, 8, 9, 10].

Exact solutions to Maxwell's equations are known only for special geometries such as spheres, spheroids, or infinite cylinder, so approximate methods are in general required. Comprehensive review of methods of analysis used in near field optics theory may be found in review papers and in monographs [11, 12, 13, 14]. Expansion of solution on multipolar eigenfunctions has been applied to many near-field optical problems in early studies [15]. Several approximate methods have been used for calculation of spatial distribution of near-field induced by external electromagnetic wave around nanoparticles of arbitrary geometrical shape in electrostatic approximation, which is applicable when size of nanoparticles is much less than wavelength of EM field. Among them most popular are discrete-dipole approximation (DDA) method or coupled dipole approximation (CDA) method [16, 17]. Weak point of DDA or CDA methods is that they can not be applied for particles with large (exceeding 2) refractive index because of its low accuracy and can not describe accurately fine structure with large field gradients.

Another approximate method commonly used for calculating distribution and enhancement of local fields is finite difference time domain (FDTD) method [18]. This method

was applied to calculate local field distribution in a junction between two silver nanoparticles [19]. This method also has disadvantage that it can not describe accurately large field gradients.

For our purposes we found out that most suitable is Boundary Charge Method (BCM) when Maxwell's equations are solved numerically using integral equation formulation [21, 22]. Below we will show that by using this method one can more accurately calculate fine structure of local field distribution in space between plasmon nanoparticles and on surfaces.

When metallic or dielectric body is exposed to the external electric field, the maximum field enhancement is achieved at the points of its surface with maximal curvature. Further field amplification is obtained by tuning the frequency of the external field towards the frequency of an appropriate surface plasmon oscillation. This is illustrated by Fig. 1, where the dependence of the frequency of the dipole plasmon resonance (a) and the maximal field enhancement (b) on the aspect ratio a/b ($a > b$) of a single prolate spheroid is depicted using the well-known solution of the Poisson equation in elliptic coordinates [24]. Here the external field is parallel to the large axis of the spheroid. In plotting Fig. 1, a simple approximation for the dielectric function of silver, $\varepsilon(\omega) = 6.4 - 100/\omega(\omega + 0.06i)$, where the frequency, ω , is measured in eV, was used [2]. As is readily seen from Fig. 1, the field enhancement for a sufficiently long body may achieve several thousands. Also, increasing aspect ratio of a spheroidal particle results in a significant red shift of the plasmon resonance.

Combining particles of various size and shape one may attempt to construct a nanolens with the region of the maximum field intensity (a hot spot or a nanofocus) located in a gap between nanoparticles apart from their surfaces. Recent computations implementing the multiple spectral expansion method [20] demonstrated the emergence of such a nanofocus in a system of self-similar chain of metallic spheres of different size. Such a possibility is very attractive since it allows for remote detection without the mechanical contact between a molecule and a nanoparticle.

The main purpose of the present paper is to investigate the field distribution near hot spots in sets of plasmon nanoparticles. In section II, a simple classification of critical points of the field intensity is given. It is shown that in electrostatic approximation when one can neglect retardation effects absolute maxima of the field intensity are impossible in space outside surfaces of nanoparticles and the only possible critical points outside surfaces are either absolute minima or saddle ones. The boundary charge method is explained in section III

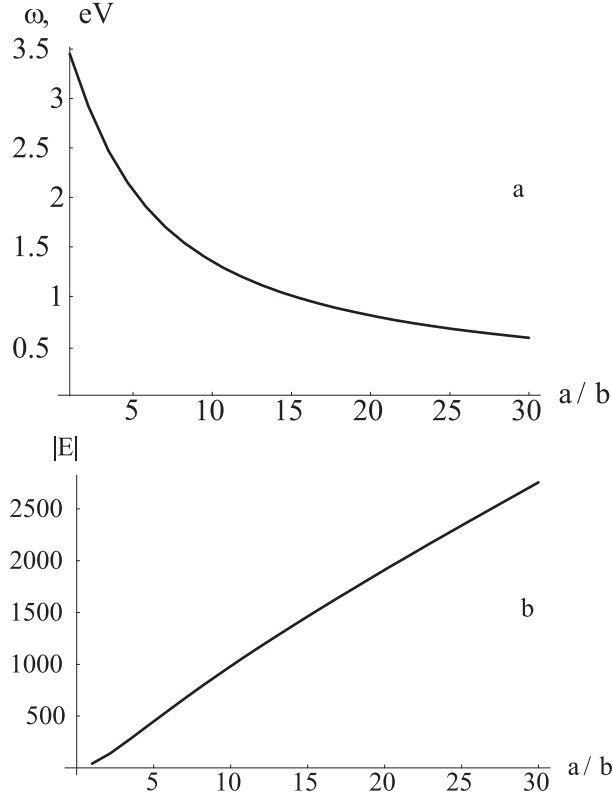


FIG. 1: The plasmon frequency (a) and the maximal field enhancement (b) versus the aspect ratio of a prolate spheroid.

and the results of numeric calculations of the near field distribution produced by symmetric star-like sets of prolate spheroids are presented in section IV. Finally, in section V the fine structure of the field distribution around a self-similar chain composed of metallic spheres [20] is investigated and it is shown that maximum field intensity is achieved on surfaces of nanoparticles. A brief summary is given in concluding section VI.

II. FIELD DISTRIBUTION NEAR CRITICAL POINTS

When dimensions of nanoparticles are much less than the wavelength of an incident electromagnetic field, one can neglect retardation effects and use the electrostatic approximation to calculate the field distribution. Thus in the near-field region, the electric field, $\mathbf{E}(\mathbf{r}) = -\nabla\varphi(\mathbf{r})$, satisfies Poisson's equation,

$$\nabla\varepsilon(\omega, \mathbf{r})\nabla\varphi(\mathbf{r}) = 0, \quad (1)$$

with the boundary condition

$$\mathbf{E}(\mathbf{r} \rightarrow \infty) \rightarrow \mathbf{E}^{in}, \quad (2)$$

where $\varepsilon(\omega, \mathbf{r})$ is the complex dielectric permittivity and \mathbf{E}^{in} is the electric field amplitude of the incident electromagnetic wave. In traditional electrostatic problems, when the dielectric permittivity is independent of ω , both the external field and the potential are real-valued functions. In application to the near-field optics, both the electric field of the incident wave, \mathbf{E}^{in} , and the potential, $\varphi(\mathbf{r})$, may be complex-valued due to the possible elliptical polarization of the incident wave and due to the energy losses inside nanoparticles.

Prior to discussing the results of numeric solution to Eq. (1), we give the qualitative description of hot spots. To be more rigorous, we define a hot spot as a point where the field intensity distribution has a maximum in certain directions. In other words, we are interested in the critical points with zero gradient, $\nabla I(\mathbf{r}) = 0$, where the field intensity is $I(\mathbf{r}) = |\mathbf{E}(\mathbf{r})|^2 = |\nabla\varphi(\mathbf{r})|^2$. The question is what kind of critical points are possible apart from the surface.

To answer this question suppose that the critical point is at the origin, $\mathbf{r} = 0$. In a vicinity of this point, the solution to Poisson equation (1) may be written as a sum

$$\varphi(\mathbf{r}) = \varphi_0 - \mathbf{E}_0 \cdot \mathbf{r} + \varphi_2(\mathbf{r}) + \varphi_3(\mathbf{r}) + \dots, \quad (3)$$

where \mathbf{E}_0 is the electric field at the origin and $\varphi_n(\mathbf{r})$ are harmonic polynomials of the order n . In particular, the quadratic and cubic parts of the expansion are

$$\varphi_2(\mathbf{r}) = A_2 \{3(\mathbf{n}_1 \cdot \mathbf{r})(\mathbf{n}_2 \cdot \mathbf{r}) - (\mathbf{n}_1 \cdot \mathbf{n}_2)r^2\}, \quad (4)$$

$$\begin{aligned} \varphi_3(\mathbf{r}) = A_3 \{ & 5(\mathbf{m}_1 \cdot \mathbf{r})(\mathbf{m}_2 \cdot \mathbf{r})(\mathbf{m}_3 \cdot \mathbf{r}) \\ & - r^2[(\mathbf{m}_1 \cdot \mathbf{r})(\mathbf{m}_2 \cdot \mathbf{m}_3) + (\mathbf{m}_2 \cdot \mathbf{r})(\mathbf{m}_1 \cdot \mathbf{m}_3) + (\mathbf{m}_3 \cdot \mathbf{r})(\mathbf{m}_1 \cdot \mathbf{m}_2)] \} \end{aligned} \quad (5)$$

where $A_{2,3}$ are arbitrary constants and $\mathbf{n}_{1,2}$ and $\mathbf{m}_{1,2,3}$ are arbitrary unit vectors. The field intensity near the origin looks like

$$I(\mathbf{r}) = E_0^2 - 2\text{Re}(\mathbf{E}_0^* \cdot \nabla\varphi_2(\mathbf{r})) + |\nabla\varphi_2(\mathbf{r})|^2 - 2\text{Re}(\mathbf{E}_0^* \cdot \nabla\varphi_3(\mathbf{r})) + \dots \quad (6)$$

Let us consider first the case of linear polarized incident wave; then \mathbf{E}^{in} in Eq. (2) is a real vector. If the losses inside dielectric particles are negligible, $\text{Im} \varepsilon(\omega) = 0$, the resulting

solution to the Poisson equation is a real-valued function. According to Eq. (6) the condition of zero intensity gradient at $\mathbf{r} = 0$ is $\mathbf{E}_0 \cdot \nabla \varphi_2 \equiv 0$. It is a matter of simple algebra to check that this yields either to $\mathbf{E}_0 = 0$ or to $A_2 = 0$ in Eq. (4). The first possibility, $\mathbf{E}_0 = 0$, corresponds to the absolute minimum of the field intensity, $I(0) = 0$; this field configuration is used in the well-known Paul traps. The second possibility means that $\varphi_2(\mathbf{r}) = 0$ in Eqs. (3,6), hence the quadratic part of the expansion in Eq. (6) is $-2\mathbf{E}_0 \cdot \nabla \varphi_3(\mathbf{r})$. The latter expression is a harmonic function. According to the well-known properties of harmonic functions [24] it cannot take maximal or minimal values inside its domain. The only possible critical points are the saddle ones. Thus, with a linear polarization of an incident wave and negligible losses the field intensity apart from the surface of dielectric bodies may be either zero at certain points or it may exhibit a saddle point.

In the case of complex-valued fields the analysis is similar but more tedious. The zero-gradient condition, $\nabla I(\mathbf{r}) = 0$, does not necessarily mean that $\varphi_2(\mathbf{r})$ in Eq. (3) vanish. In order to classify the critical points of the field intensity we have to investigate the eigenvalues of the quadratic form $I_2 = |\nabla \varphi_2(\mathbf{r})|^2 - 2\text{Re}(\mathbf{E}_0^* \cdot \nabla \varphi_3(\mathbf{r}))$ appearing in Eq. (6). Since all coefficients and vectors entering in Eqs.(4,5) are generally complex, the quadratic form I_2 depends on 12 complex numbers. We have studied the signature of I_2 using Mathematica 5.0 symbolic software. It was found that three eigenvalues are never negative all at once, that is, the field intensity (6) never takes maximal value apart from dielectric surfaces. The signature of the quadratic form, I_2 , may be either $(+, -, -)$, $(+, +, -)$ or $(+, +, +)$. The latter possibility corresponds to the local minimum of the field intensity that may now exist even if $\mathbf{E}_0 \neq 0$. Although such a ‘‘cold spot’’ is hardly of use in the near-field optics, it is worth writing down a corresponding example of the field distribution:

$$\varphi(\mathbf{r}) = -x + 2y + z + 2ixy + \frac{1}{8}x^2y - \frac{1}{4}y^3 + \frac{1}{4}x^2z + \frac{1}{4}xyz - \frac{1}{4}y^2z + \frac{5}{8}yz^2 \quad (7)$$

Thus the most important conclusion from this analysis is that the field intensity cannot take maximal values apart from the dielectric surfaces. The spatial distribution of the intensity may exhibit either saddle points or minima. Below we demonstrate several numeric examples with both types of saddle points.

III. BOUNDARY CHARGE METHOD

For the case of materially equal dielectric particles the problem is conveniently reduced to a set of integral equations for the surface charge density, σ , induced at the nanoparticles [21] or, equivalently, for the surface distribution of the normal electric field [23]. Compared to various direct methods of the numeric solution of Eq. (1), the integral equation approach allows to reduce dimensionality of a problem and to achieve reasonable accuracy at smaller computer cost. Here, we use the boundary charge method (BCM) based on the integral equations in the form derived in [21]:

$$\Lambda(\omega)\sigma(\mathbf{s}) = -\mathbf{n}(\mathbf{s}) \cdot \mathbf{E}^{in}(\mathbf{s}) + \int ds' F(\mathbf{s}, \mathbf{s}')\sigma(\mathbf{s}'), \quad (8)$$

where

$$\Lambda(\omega) = 2\pi \frac{1 + \varepsilon(\omega)}{1 - \varepsilon(\omega)}, \quad (9)$$

and

$$F(\mathbf{s}, \mathbf{s}') = -\frac{\mathbf{n}(\mathbf{s}) \cdot (\mathbf{s} - \mathbf{s}')}{|\mathbf{s} - \mathbf{s}'|^3}. \quad (10)$$

The integration in Eq. (8) is carried over the multiply connected surface of all particles, vectors \mathbf{s} and \mathbf{s}' belong to the surface, and $\mathbf{n}(\mathbf{s})$ stands for the surface unit normal directed towards vacuum at \mathbf{s} . Once Eq. (8) is solved and the surface charge distribution, $\sigma(\mathbf{s})$, is found one can calculate the induced electric field at the arbitrary point outside the surface using a simple formula

$$\mathbf{E}(\mathbf{r}) = \mathbf{E}^{in} - \nabla_{\mathbf{r}} \int ds \frac{\sigma(\mathbf{s})}{|\mathbf{r} - \mathbf{s}|}. \quad (11)$$

Eq. (8) was approximated by a set of linear equations with the help of an appropriate triangulation of the surfaces. Our computer facilities allowed us to use up to 5000 triangulation points. As a test problem, we investigated the dipolar plasmon resonance for a single prolate spheroid. Comparing the numeric solution with the well-known analytic expressions (see fig. 1), it was found that with the maximum affordable number of triangulation points the accuracy within 10% is achieved for the spheroid aspect ratio not exceeding 6 : 1.

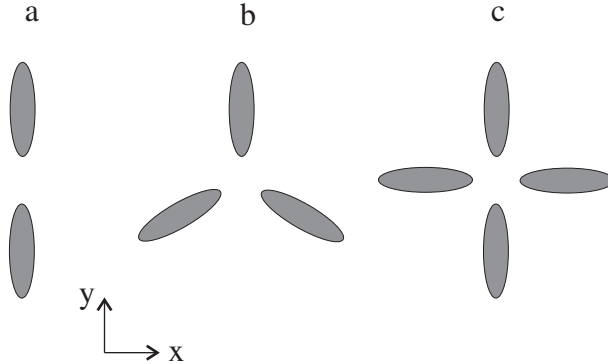


FIG. 2: Sets of prolate spheroids used in computations.

IV. RESULTS OF COMPUTATIONS FOR STAR-LIKE SETS OF NANOPARTICLES

Now we turn to the discussion of the numeric solutions to integral equation (8). We have investigated the field structure near the sets of prolate spheroids (Fig. 2). For the examples discussed below, the aspect ratio of all spheroids is 4 : 1, their centers are at $r = 4.5$ from the origin. The complex dielectric permittivity, $\varepsilon(\omega)$, corresponds to silver.

Fig. 3 shows the dependence of the field enhancement, $f = |\mathbf{E}|/|\mathbf{E}^{in}|$, at the origin on the frequency of the incident wave for the configuration depicted in Fig. 2a. The incident wave propagating along the z axis is linear polarized with the electric field vector along the y axis, $\mathbf{E}^{in} = (0, 1, 0)$. The field distribution along y axis is also shown. The electric field here is maximal at the surfaces of spheroids. At the origin, there is the maximum in zx plane and the minimum in y direction. The signature of the saddle point at $\mathbf{r} = 0$ is $(-, +, -)$. Notice that the maximum field enhancement for a single 4 : 1 prolate spheroid is about $f \approx 300$ (fig. 1), that is, the maximum field at the origin is approximately half as much. With the circular polarization of the incident wave, there are just minor changes in the field structure.

More complicated behavior is observed for the star composed of three spheroids (Fig. 2b). Fig. 4a shows the field versus the frequency for the circular polarization of the incident wave, $\mathbf{E}^{in} = (1, i, 0)/\sqrt{2}$. The plasmon resonance frequency (2.42 eV) in this case is a little red-shifted compared to two spheroids (2.44 eV). The field structure, however, is entirely different. The field distribution along the y axis is depicted in Fig. 4b. The two-dimensional contour plot of the field intensity is shown in Fig. 5, where the the electric field vectors are also plotted.

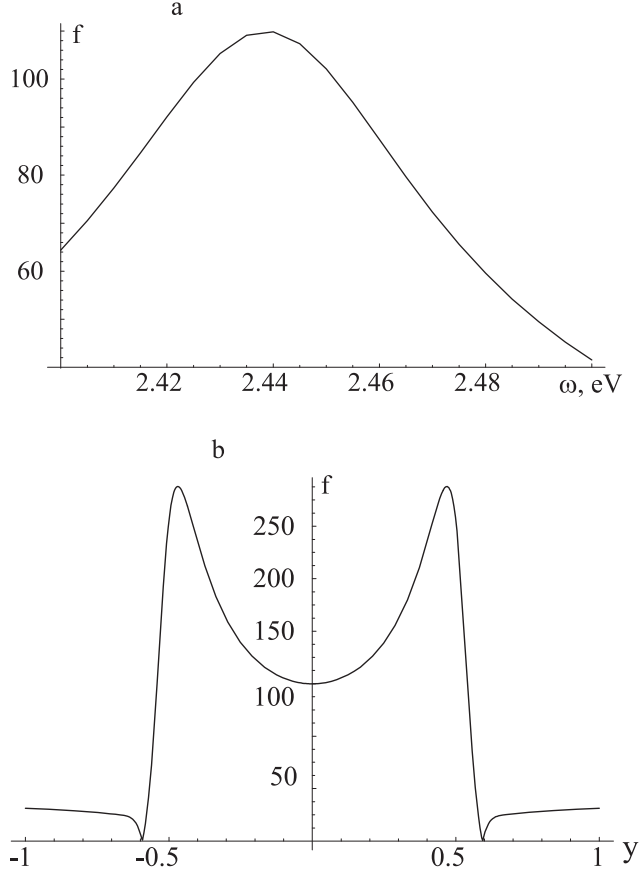


FIG. 3: (a) — The field at the origin versus frequency of the incident wave, (b) the field distribution along the y axis ($\omega = 2.44$ eV) for the set shown in Fig. 2a.

Instead of a single saddle point between two spheroids now there are four critical points. The minimum in the xy plane (marked with the \times sign in Fig. 5) is situated at the origin. Three others (\circ) are maximums in the radial direction and minimums in the azimuthal direction. The field enhancement at these points is about $|\mathbf{E}| \approx 150$. Fig. 5 also shows the real and imaginary parts of the electric field vector. As is readily seen, the ellipticity of the wave is essentially nonuniform, i.e., this set of spheroids acts as a polarizer.

In contrast with two spheroids, the field structure in the 3-star is sensitive to the polarization of the incident wave. Fig. 6 shows the intensity distribution and the electric field for the linear polarization of the incident wave, $\mathbf{E}^{in} = (0, 1, 0)$. Now there are only two $(+, -, -)$ saddle points with the field enhancement $|\mathbf{E}| \approx 130$. Besides, the $(+, +, -)$ point moves to the lower part of the figure.

Similar behavior was observed for the structures consisting of larger number of prolate

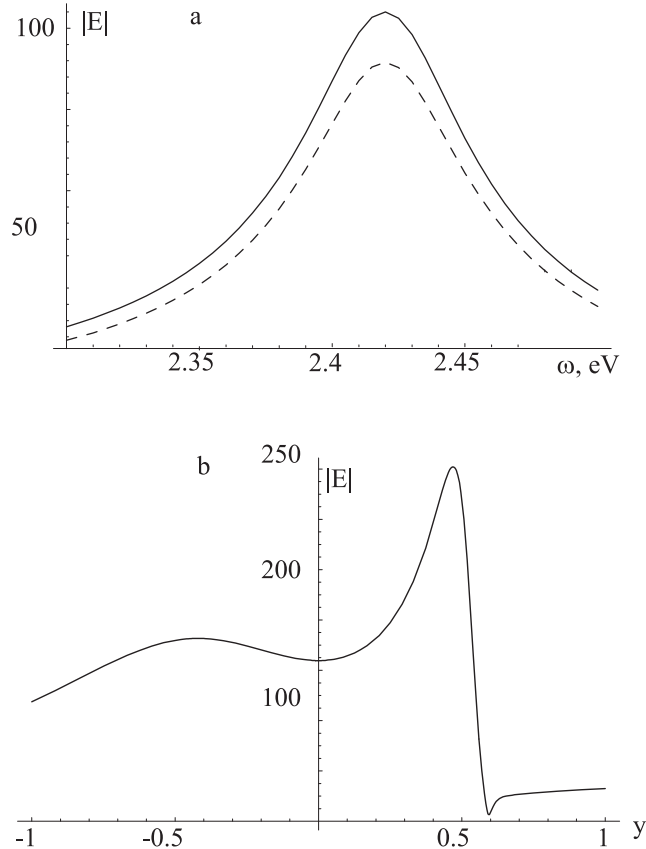


FIG. 4: a — Field amplitude versus frequency for the circular polarization of the incident wave and configuration depicted in Fig. 2b. Solid line — $\mathbf{r} = (0, -0.45, 0)$, dashed line — $\mathbf{r} = (0, -0.45, 0)$. b — Field distribution along y axis.

spheroids. Fig. 7a shows the plasmon resonance for the circular polarization of the incident wave. The field distribution along a line coming through the gap between two adjacent spheroids is depicted in fig. 7b. The two-dimensional plot (Fig. 8) demonstrates a single $(+, +, -)$ saddle point and four $(+, -, -)$ saddle points.

V. FIELD ENHANCEMENT BY A SELF-SIMILAR CHAIN OF SPHERES

As we have already mentioned, it was recently proposed to achieve larger field enhancement implementing self-similar sets of nanoparticles [20]. The idea is based on the fact that in the near-field region the field enhancement is independent of absolute size of particles. Therefore, if there two spheres of different size separated by a small gap, then the resulting field enhancement at smaller sphere should be about f^2 , where f is the enhancement factor

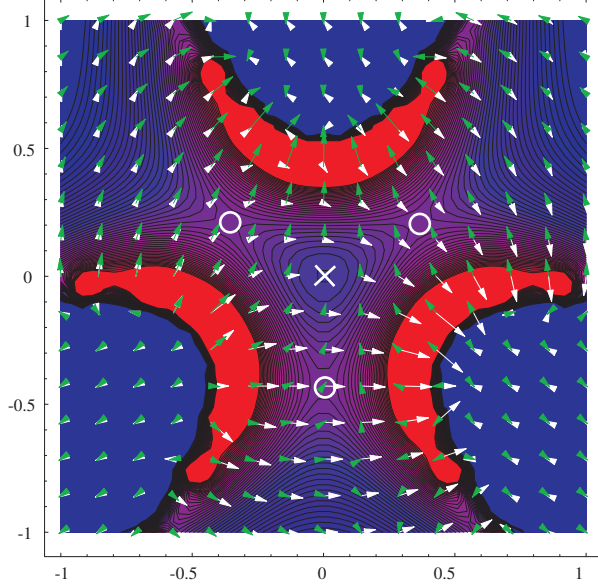


FIG. 5: Field distribution in xy plane around three spheroids (Fig. 2b) with circular polarization of the incident wave. \times corresponds to $(+, +, -)$ saddle point, \circ corresponds to $(+, -, -)$ saddle points. Green arrows — $\text{Re } \mathbf{E}$, black arrows — $\text{Im } \mathbf{E}$.

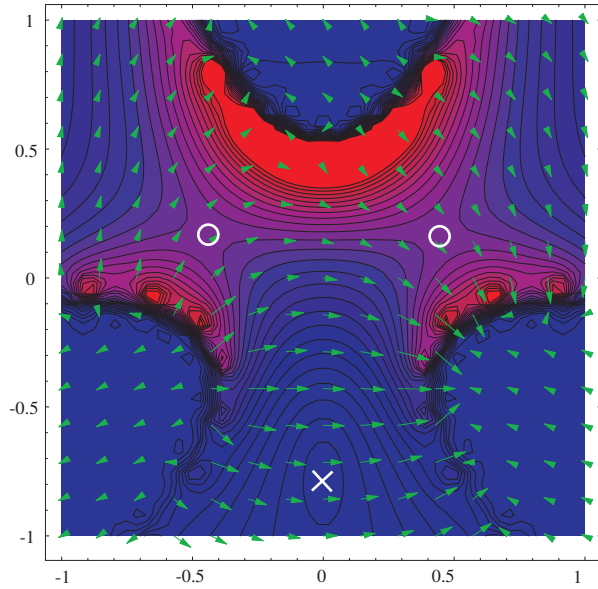


FIG. 6: Same as in Fig. 5 but with linear polarization of the incident wave.

for a single isolated sphere, which depends on its material only. Combining m spheres of reducing radii one may expect to achieve the electric field at the surface of the smallest sphere enhanced by a factor of f^m .

We used BCM to investigate a combination of three silver spheres studied in [20]. The

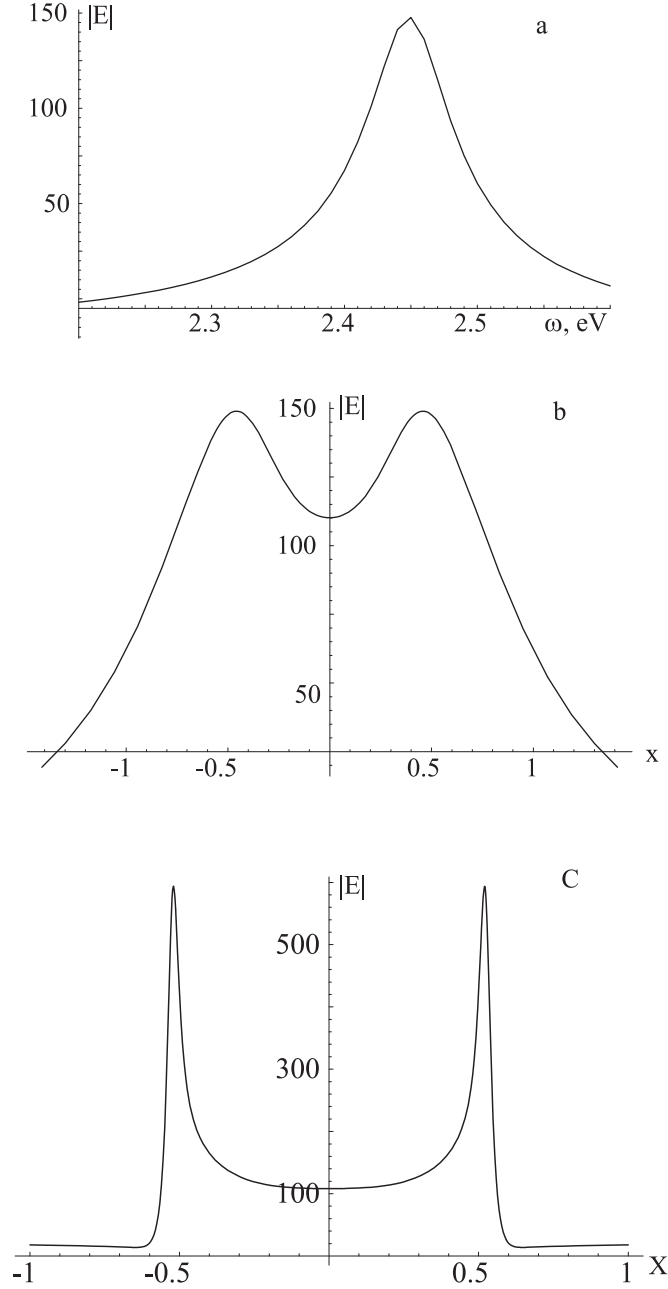


FIG. 7: a — Field amplitude versus frequency for the circular polarization of the incident wave for the set shown in fig. 2c. b — Field distribution along the $y = x$ line. c — Field distribution along the x axis.

radii of spheres are $R = 1, 1/3, 1/9$, their centers are at $z = 0, 1.53, 2.0$. The electric field of the incident wave is parallel to the z axis. The field distribution along the z axis is depicted in Fig. 9. As is readily seen from the figure, the field at the surface of the smallest sphere is really enhanced by a factor of 600. However, the maximal field is achieved rather

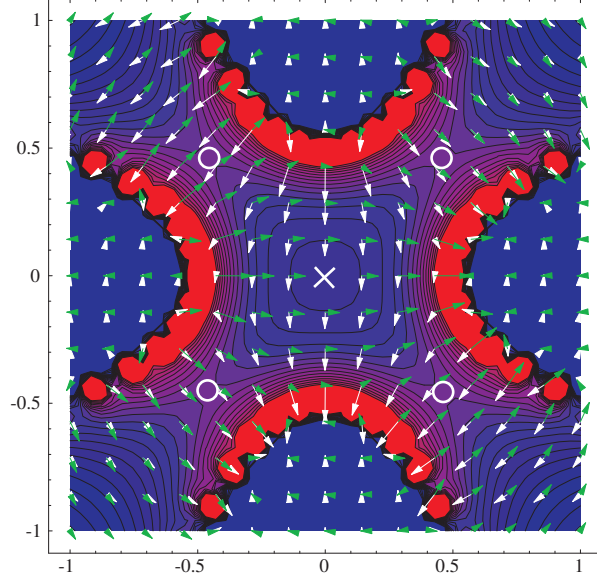


FIG. 8: Same as in Fig. 5 for the 4-star set (Fig. 2c).

at the surface of the sphere then in a gap between spheres (see Fig. 9b, where the magnified part of Fig. 9a is shown).

VI. CONCLUSION

It is shown that in the nonretarded approximation the absolute maximum of the field intensity distribution around dielectric bodies illuminated by an external source is achieved at the surface. The only possible critical points of the intensity distribution outside surfaces are either saddle or minimal points. The computed field distribution around the sets of prolate spheroids having the aspect ratio factor up to 4 exhibits the maximum field enhancement on the order of 300 at the points of the surface with maximal curvature. It is worthy to note, that the field enhancement provided by a single silver sphere is about 30 [19]. However, in star like set of nanoparticles the field enhancement at the saddle points ("hot spots") outside the surfaces is also sufficiently large, $f \approx 150$. even for the aspect ratio 4. Since the Raman scattering is proportional to the fourth power of the electric field, the corresponding Raman cross-section is enhanced by a factor of $5 \cdot 10^8$. Preliminary computations with the increased aspect ratio and the fixed distance between spheroids demonstrated, first, the significant red shift of the plasmon resonance. Second, the field enhancement at the saddle points is approximately half the enhancement at the tip of an single spheroid with the same aspect

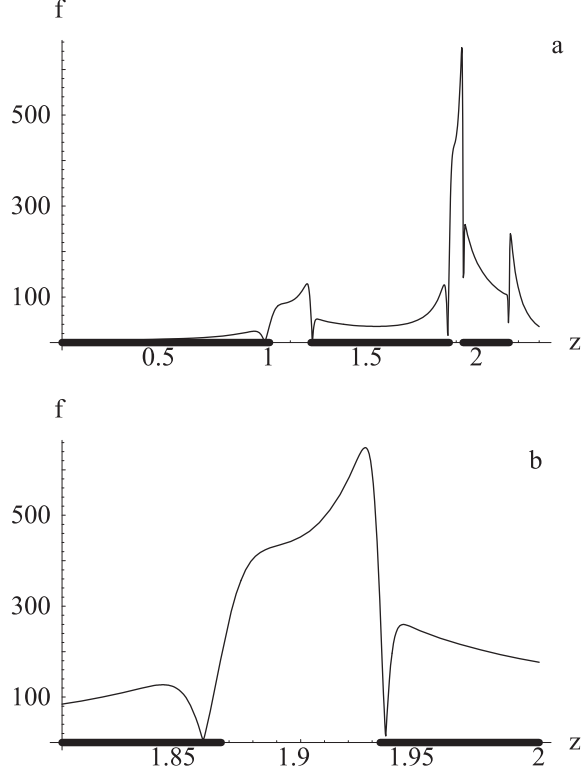


FIG. 9: Field distribution along a chain composed of three silver spheres, $\omega = 3.35eV$. Heavy lines mark the position of the spheres.

ratio, that means, that field amplification at central points may achieve a value of several thousands for the aspect ratio of spheroids in a range 20-25 according to scaling law for isolated spheroidal shape particle presented on Fig. 1. That means that one could expect amplification of Raman cross section for molecule placed in the focus of star-like nanolens to achieve as much as 10^{14} or even more. This may open possibility of the single molecule Raman spectroscopy in the scanning mode in an AFM type device with nanolens placed on the tip of AFM.

The polarization state of the incident electromagnetic field is also of importance. Qualitatively, the circular polarized wave may be represented as a sum of linear polarized waves with different directions of the electric field and appropriate phase shifts. In the symmetric configurations like those shown in Fig. 2, each wave excites its own spheroid. The field

distributions depicted in Figs. 4,7 appear as a result of interference.

- [1] D. W.Pohl and D. Courjon, Eds. *Near Field Optics*, NATO ASI, Series E: Applied Sciences - vol 242, Kluwer Academic Publishers (1993)
- [2] U. Kreibig and M. Vollmer, *Optical Properties of Metal Clusters*, Springer-Verlag, Berlin (1995)
- [3] A.M. Michaels, M. Nirmal, and L.E. Brus, *J. Am. Chem. Soc.*, **121**, 9932 (1999)
- [4] J. Jiang, K. Bosnick, M.Maillard, and L.E. Brus, *J. Phys. Chem., B*, **107** 9964 (2003)
- [5] M. Moskowits, *Rev. Mod.Phys.*, **57** 783 (1985)
- [6] A. Wokaun, *Solid State Physics*, **38** 223 (1984)
- [7] G. C. Schatz, R.P. Van Duyne in *Handbook of Vibrational Spectroscopy*, J.M. Chalmers and R.P. Griffiths (Eds), Wiley & Sons, Ltd, New Yourk, 2002, vol.1, pp 759-774
- [8] K. Kneipp, Y.Wang, H. Kneip *etal.*, *Phys. Rev. Lett.*, **78**, 1667 (1997)
- [9] S. Nie, S. R. Emory, *Science*, **275** 1102 (1997)
- [10] H. Xu, E. J. Bjerneld, M. Kaell, L. Borjesson, *Phys. Rev. Lett.*, **83**, 4357 (1999)
- [11] C. Girard and A. Dereux, *Rep. Prog. Phys.* **59** 657 (1996).
- [12] S. Kawata, M. Ohtsu, and M. Irie (Eds), *Nano-Optics*, Springer-Verlag (2002).
- [13] M. Ohtsu (Ed.), *Near-Field Nano/Atom Optics and Technology* Springer-Verlag, Tokyo, Berlin (1998).
- [14] M. Ohtsu, K. Kobayashi, *Optical Near Fields*, Springer-Verlag (2004)
- [15] L. Novotny, D. Pohl, *at al*, *J. Opt.Soc. Am.*, **A11**, 1768 (1994)
- [16] B.T. Draine *et al*. *Journ Opt.Soc. Am.*, **11A** 1491 (1994).
- [17] K.L. Kelly *et al*, *J. Phys. Chem. B.*, **107** 668 (2003).
- [18] A.Taflove and S. C. Hagness, *Computational Electrodynamics: The Finite-Difference Time-Domain Method* , Artech House, Boston (2000).
- [19] M. Futamata, Y. Maruyama, M. Ishikawa, *J. Phys. Chem. B* **107** 7607 (2003).
- [20] K. Li, M.I. Stockman, and D.J. Bergman, *Phys. Rev. Lett.*, **91**, 227402 (2003).
- [21] F.J. García de Abajo, J. Aizpurua, *Phys. Rev. B*, **56**, 15873 (1997).
- [22] H. Xu, J. Aizpurua, M. Kall, and P. Apell, *Phys. Rev. E.*, **62**, 4318 (2000).
- [23] A. Ignatov, *P.N. Lebedev Inst. Rep.*, #5 (1982)

[24] P.M. Morse, H. Feshbach, *Methods of Theoretical Physics* New-York, McGraw-Hill (1953)